ISSN 0029-3865

CBPF-NF-046/88

QUANTITATIVE ANALYSIS OF COSMOLOGICAL MODELS IN A BRANS-DICKE THEORY

by

C. ROMERO[+], H.P. OLIVEIRA[§]* and J.R.T. de MELLO NETO[1]**

[1]Centro Brasileiro de Pesquisas Físicas - CBPF/CNPq
Rua Dr. Xavier Sigaud, 150
22290 - Rio de Janeiro, RJ - Brasil

[+]Departamento de Física
Universidade Federal da Paraíba
58050 - João Pessoa, PB - Brasil

[§]Instituto de Física
Universidade do Estado do Rio de Janeiro
20271 - Rio de Janeiro, RJ - Brasil

*Work partially support by CNPq (Brazil).

ABSTRACT

Isotropic and homogeneous cosmological models with a perfect fluid source in Brans-Dicke theory are investigated from the point of view of dynamical system theory.

Key-words: Brans-Dicke theory; Dynamical system; Cosmological solutions.

Introduction

The attempts of incorporating Mach's principle into a relativistic theory of gravity ,as well as the introduction of a time dependence for the Newtonian gravitation constant ,have made Brans-Dicke theory (BDT) quite appealing to a wide class of cosmologists since it appeared in 1961[1]. The fact that present observational data still do not make a conclusive choice between this theory and general relativity seems to give BDT a privileged status among other alternative theories of gravitation[2].At the same time,a growing theoretical research in the direction of the so called scalar-tensor theories (of which BDT is ,certainly,the most interesting case) is being carried out in recent years. As an example of this renewed interest,we can quote the important role BDT begins to play in the context of inflationary universe program and supergravity[3,4].

In this paper we investigate homogeneous and isotropic cosmological models in Brans-Dicke theory from the point of view of dynamical systems.Restricting ourselves to line elements of Friedmann-Robertson-Walker type with zero-spatial curvature (k=0) and considering as sources perfect fluids with an equation of state of the form $p=\lambda\rho$ $(0\leq\lambda\leq 1)$,we can reduce the field equations to a two-dimensional autonomous dynamical system .Projecting the phase portraits of this system on the Poincaré's sphere[5] ,we are left with a general picture of the solutions which permit us to study their behavior at infinity,the existence of cosmological singularities,stability of Minkowski's spacetime ,etc.Our approach consists basically of taking arbitrary values for the coupling constant w and regarding fluids obeying different equations of

state according to the value chosen for λ.

In order to get a complete knowledge of the evolution of the dynamical system as a function of the coupling constant, we have made computations for several values of w. As a matter of fact, the correct value of w which should appear in Brans-Dicke equations is not known yet. Nevertheless, theoretical arguments and experimental results put some restrictions on its domain of validity or even predict specific numbers to be assigned to it. For example, if we consider, as in Dickes's revised version[6], an energy-momentum tensor $T_{\mu\nu}(\phi)$ containing the scalar field ϕ of BDT, then the strong energy condition $T_{\mu\nu}V^{\mu}V^{\nu} \geq T/2$ constrains the value of w to be greater than $-3/2$[7,8]. To account for the perihelium motion of Mercury, on the other hand, w has to be set greater than 6[9,10]. Furthemore, to avoid a possible violation of the gravitational weak equivalence principle some authors require a lower limit on the coupling constant of w = 29[11]. At this point, it is worth mentioning that as w becomes larger, Brans-Dicke theory turns out to be observationally indistinguishable from general relativity. This conclusion is not unexpected since in the limit $w \to \infty$ and $\phi = G^{-1}$ Brans-Dicke field equations become identical to the Einstein equations of general relativity theory.

1. The field equations

The general Brans-Dicke equations may be written as

$$R_{\mu\nu} = -(8\pi/\phi)\left[T_{\mu\nu} - \left(\frac{w+1}{2w+3}\right)Tg_{\mu\nu}\right] - \frac{w}{\phi^2}\phi_{;\mu}\phi_{;\nu} - \frac{1}{\phi}\phi_{;\mu;\nu} \qquad (1.a)$$

$$\Box\phi = \frac{8\pi T}{2w+3}\,, \qquad (1.b)$$

where $T_{\mu\nu}$ and T denote the energy-momentum tensor and its trace, respectively , which represent the matter content of the universe. For perfect fluids $T_{\mu\nu} = \rho V_\mu V_\nu - p h_{\mu\nu}$, $h_{\mu\nu}$ being the projection tensor in the subspace orthogonal to the 4-velocity vector field V_μ , ρ the energy density and p the thermodynamic pressure.

Now, let us consider a Friedmann-Robertson-Walker metric with euclidean spatial sections written in the standard form

$$ds^2 = dt^2 - R^2(t)[d\chi^2 + \chi^2(d\theta^2 + \text{sen}^2\theta d\phi^2)].$$

The assumption of homogeneity and isotropy requires the scalar field to be time-dependent only ,i.e., $\phi = \phi(t)$. Thus, in a co-moving coordinate system ($V^\mu = \delta^\mu_0$), Brans-Dicke equations (1.a) and (1.b) for a perfect fluid satisfying an equation of state $p = \lambda\rho$ are:

$$\dot{\theta} + \frac{\theta^2}{3} = - \frac{8\pi\rho}{\phi}\left[1 - \frac{w+1}{2w+3}(1-3\lambda)\right] - w\frac{\dot{\phi}^2}{\phi^2} - \frac{\ddot{\phi}}{\phi} \qquad (2.a)$$

$$\frac{\dot{\theta}}{3} + \frac{\theta^2}{3} = - \frac{8\pi\rho}{\phi}\left[\lambda + \frac{w+1}{2w+3}(1-3\lambda)\right] - \frac{\theta}{3}\frac{\dot{\phi}}{\phi} \qquad (2.b)$$

$$\ddot{\phi} + \theta\dot{\phi} = \frac{8\pi\rho}{2w+3}(1-3\lambda) \ , \qquad (2.c)$$

where $\theta = \frac{3\dot{R}}{R}$ is the expansion factor of the universe and dot means differentiation with respect to time.

Defining $\psi = \frac{\dot{\phi}}{\phi}$ and eliminating ρ from (2.c) we readily obtain the following set of first-order differential equations:

$$\dot{\theta} = F_{\lambda\omega}(\theta, \phi) \qquad (3.a)$$

$$\dot{\psi} = H_{\lambda w}(\theta, \phi), \qquad (3.b)$$

where $F_{\lambda\omega}$ and $H_{\lambda\omega}$ are given by

$$F_{\lambda\omega}(\theta,\psi) = \frac{1}{2w+3}\left[-(2+w+\lambda w)\theta^2 + \frac{3w}{2}(\lambda w - w - 1)\psi^2 + w(1-3\lambda)\theta\psi\right]$$

$$H_{\lambda\omega}(\theta,\psi) = \frac{1}{2w+3}\left[\frac{(1-3\lambda)}{3}\theta^2 - \frac{(6+5w-3\lambda w)}{2}\psi^2 - (2w+2+3\lambda)\theta\psi\right] .$$

The variable ψ defined above deserves some comments. Recalling that in Brans-Dicke theory ϕ is taken equal to the reciprocal of G ($\phi = G^{-1}$), we verify that $\psi = -\frac{\dot{G}}{G}$ and, thus, it is a mesure of the negative variation of the gravitational constant with time[1].

1. Qualitative Analysis of the dynamical system

The system of differential equations expressed by (3.a) and (3.b) is a kind of system usually referred to as a homogeneous autonomous planar system of second degree. Many of the generic features of the integral solutions of this system may be studied without working out explicit solutions $\theta = \theta(t)$ and $\psi = \psi(t)$. In fact, what really matters here is the global behaviour of classes of solutions and the stability of the equilibrium points.

The functions $F_{\lambda\omega}(\theta,\psi)$ and $H_{\lambda\omega}(\theta,\psi)$, which are quadratic homogeneous polynomials in the pair of variables $(\theta,\psi,)$, coontain λ and w as parameters which may vary according to the equation of state of the fluid and to the value chosen for the coupling constant.

To find the equilibrium points of the dynamical system (3.a)-(3.b) amounts to set simultaneously $F_{\lambda\omega}(\theta,\psi)$ and $H_{\lambda\omega}(\theta,\psi)$ equal to zero. The origin of the phase plane ($\theta = 0, \psi = 0$) turns

1 As far as variations of the gravitational constant are concerned, ψ is the natural variable to be considered. Estimations of the present value of ψ are found in the literature. See, for example, ref. (12).

out to be an equilibrium point for all values of λ and w ,and, in fact,the only significant finite equilibrium point of the system . This point corresponds to a solution which represents Minkowski's spacetime,naturally satisfying Brans-Dicke equations provided we take $\phi = G^{-1} =$ constant.[2]

Homogeneous system of the type we are dealing with are much better understood if we perform the well-known transformation of the phase plane into the Poincaré sphere.(For a complete treatment of the subject we refer the reader to ref[14].

2.Regions of negative energy density and unphysical solutions

Restrictions on the integral curves filling up the phase diagrams (to be exhibited in the next section) may be imposed by reasonable physical assumptions. One of these lies on the fact that solutions located in regions where $\rho < 0$ should not be regarded as physically admissible,at least classically.

From the system of equations(2.a) ,(2.b) and (2.c) it is possible to derive the following equation:

$$\frac{8\pi\rho}{\phi} = \theta\psi - \frac{w\psi^2}{2} + \frac{\theta^2}{3} \qquad (4)$$

This equation provides a way of detecting the sign of the energy density and,thus,allow us to rule out regions of the

[2] When $w = -4/3$ there exists an entire line of multiple equilibrium points in the phase plane. Each point (θ_0,ψ_0) of this line lies on the straight line $\psi = -\theta$ and constitutes a solution of the dynamical system (3) ($\theta = 0$, $\psi = 0$) which represents de Sitter universes with a varying gravitational constant. These special solutions were found first by O'Hanlon and Tupper[13] and , are in fact,the only de Sitter-Type solutions of Brans-Dicke equations with metric of the form we are considering. We do not construct here the phase diagram for this value of w. Also, in what follows, we exclude of our discussion the case $w = -3/2$.

diagrams in which ρ is negative. Here, we should remark two points: the first is that the existence and shape of forbidden regions do not depend upon the equation of state of the fluid; the second point is expressed by the fact that there exists a certain value $w_o = -3/2$, such that for values of the coupling constant less than w_o we have no region with negative energy density. When $w > -3/2$ there appear regions in which $\rho < 0$, and, in fact, these regions are delimited by the invariant rays which lie on the lines BB' and CC'. As the value of w increases, the classically admissible solutions tend to be confined into a narrow region containing the θ-axis (see figs. 1, 2, 3).

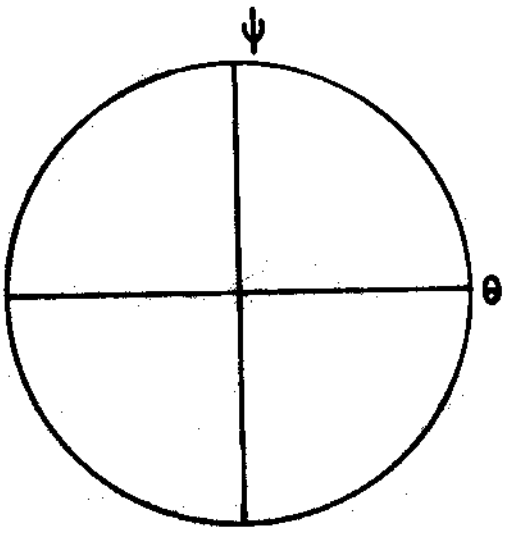

Fig. 1. There is no region with $\rho<0$ when $v<-3/2$.

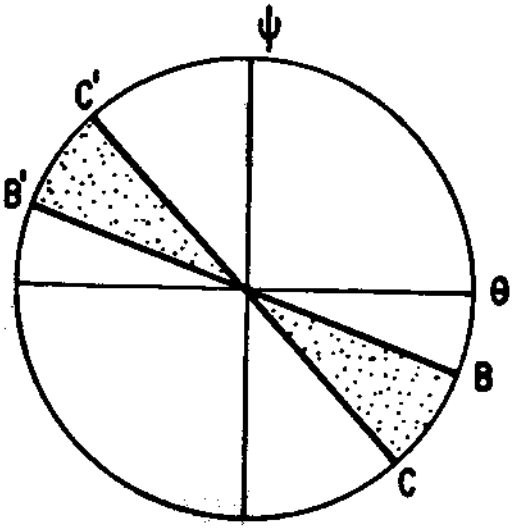

Fig. 2. Regions with $\rho<0$ (dotted). Case $(-3/2<v<0)$.

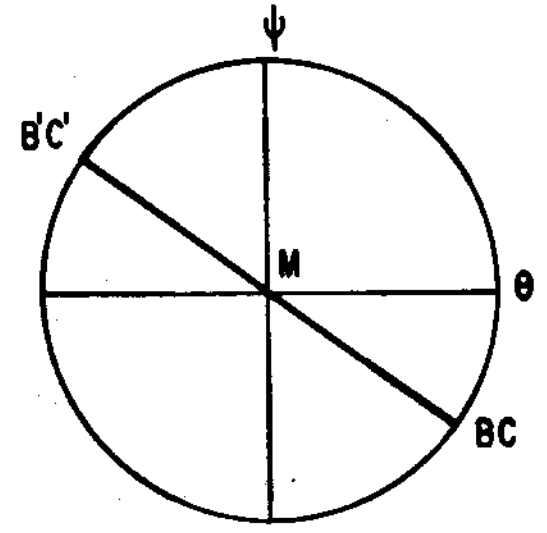

Fig.4. $W = -3/2$

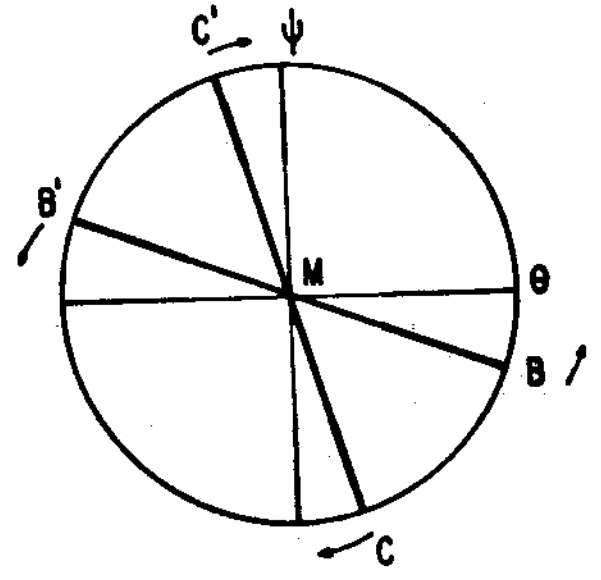

Fig.5. $-3/2 < W < 0$

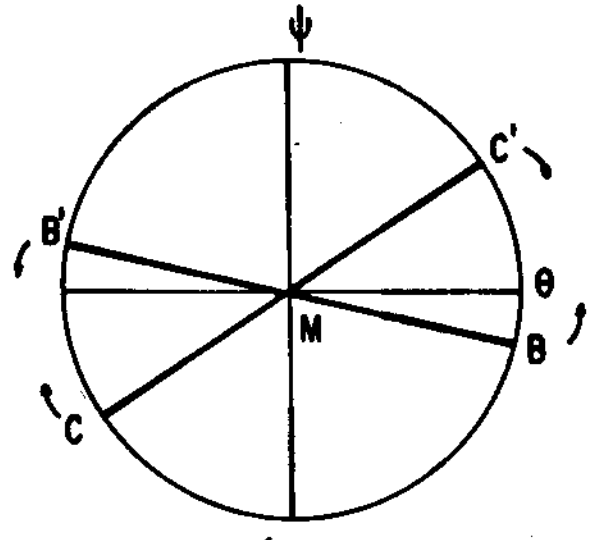

Fig.6. $W > 0$

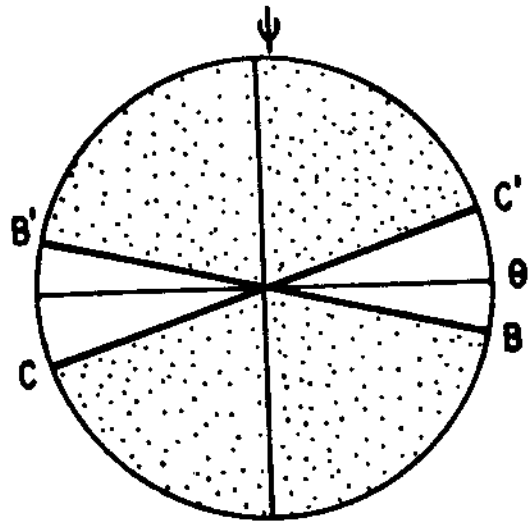

Fig. 3. Regions with $\rho<0$ (dotted) when v is positive

3. The Invariant rays of the dynamical system

Throughout the analysis of the diagrams to be presented further we will be faced with some solutions in which the ratio ψ/θ is constant. Solutions of this form are special because, in most theories where one does have a varying G, this variation occurs at a rate $\dot{G}/G = -fH$, H being the Hubble parameter and f a dimensionless number of the order of the unity[2,9]. These solutions will be referred to as the invariant rays of the dynamical system (3)[14]. In the phase plane $\theta\psi$ the invariant rays lie on straight lines and begin or end at the origin M(0,0). It turns out that when $w < -3/2$ we have two invariant rays, and when $w > -3/2$ there are six invariant rays (see appendix). The angles the invariant rays make with the θ-axis depend on w and two of them depend on λ also. If we assign a fixed value of λ to the

equations (3) , then as w varies things happen as though we had rotations of the invariant rays in the phase plane (or,on the Poincaré sphere). The four invariant rays which are independent of λ will lie on the lines BB' and CC'(see figs.4,5,6) and they do not exist if w < -3/2. When w = -3/2 ,AA',BB' and CC' all coincide making an angle with the θ-axis of -33,69°. As w increases BB' rotates in a conterclockwise sense , approaching the θ-axis. CC', in turn ,rotates in clockwise sense, tending to make an angle of -360° with the positive direction of the θ-axis. Finally, when w → +∞ , then the three lines AA', BB'and CC' tend to align with the θ-axis , AA' lying always between BB' and CC'.

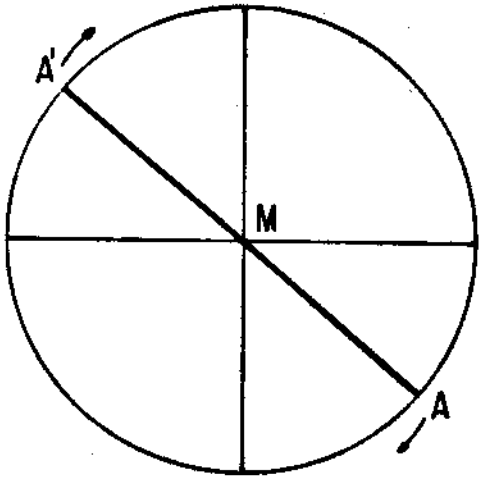

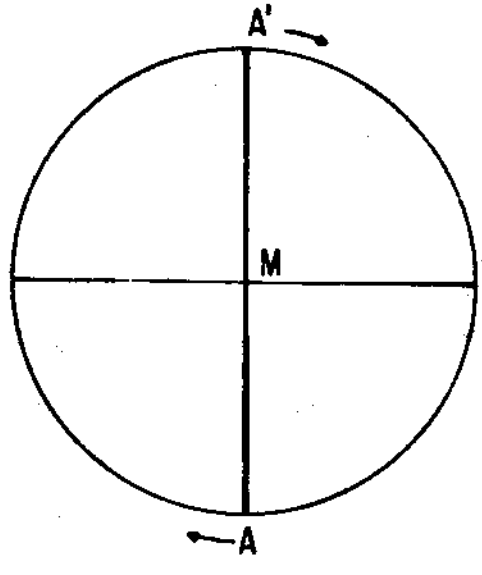

Fig. 7. $0<\lambda<1/3$ and $w<\frac{1}{\lambda-1}$

Fig. 8. $0<\lambda<1/3$ and $w=\frac{1}{\lambda-1}$

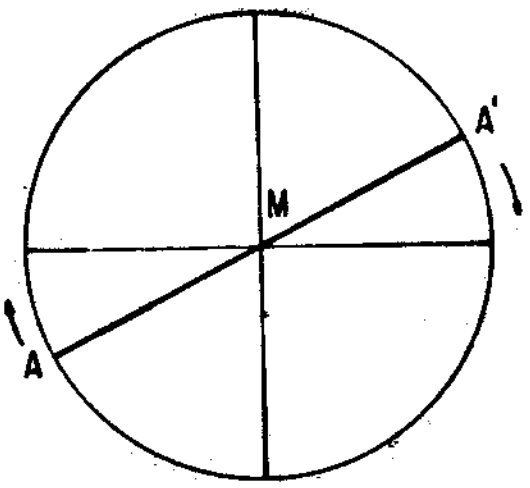

Fig. 9. $0<\lambda<1/3$ and $v>\frac{1}{\lambda-1}$

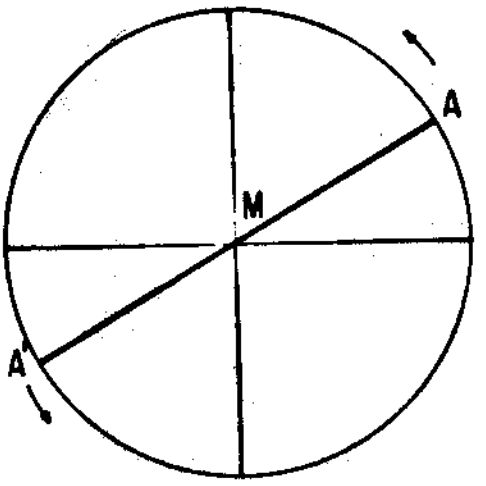

Fig. 10. $1/3<\lambda<1$ and $v<\frac{1}{\lambda-1}$

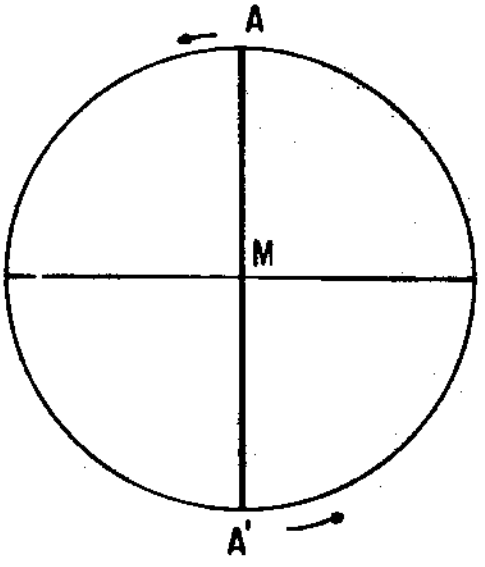

Fig. 11. $1/3<\lambda<1$ and $v=\frac{1}{\lambda-1}$

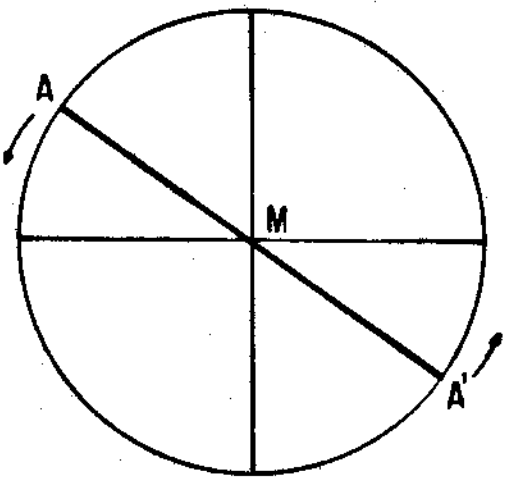

Fig. 12. $1/3<\lambda<1$ and $v>\frac{1}{\lambda-1}$

The two invariant rays ,which depend on λ and which are present for any value of w , lie on the line AA' and rotates in clockwise sense if $\lambda < -3/2$, or in counterclockwise sense if $1/3 < \lambda < 1$. For $\lambda = 1/3$ it is fixed ,making an angle of $-33,69^{\circ}$ with the positive direction of the θ-axis (see figs.7-12).

4. Representation of Brans-Dicke cosmological solutions on the Poincare' sphere (The phase diagrams).

In this section we present the phase diagrams drawn on the Poincaré sphere corresponding to fluids with the equation of state $p = \lambda\rho$, with λ varying through the following intervals: a) $\lambda=0$ (dust), b) $0<\lambda<1/3$, c) $\lambda=1/3$ (radiation), d) $1/3<\lambda<1/2$, e) $1/2\leq\lambda<1$ and f) $\lambda=1$ ('stiff matter').

a) *The dust case.*

We begin by considering a pressureless fluid, i.e., $\lambda = 0$. Essentially, we have three topologically distinct diagrams, which must be analysed separately, according to whether $w < -3/2$, $-3/2 < w < -4/3$ or $w > -4/3$. The case $w = 0$ is also analysed since it possesses some special features.

The first diagram of the dust case to be analysed refers to values of w less than $-3/2$. So, let us examine the fig.13.

The curves appearing in this diagram are, naturally, solutions of the dynamical system (3) with $\lambda=0$. They describe the evolution of cosmological models as the cosmic time goes by. Any solution of (3) for $\lambda=0$ and $w < -3/2$ must be represented by one of these trajectories. The points lying exactly on the circunference represents the infinity of the phase plane $\theta\psi$,through the well

known Poincaré mapping (see,for example,ref[5]). The origin M,

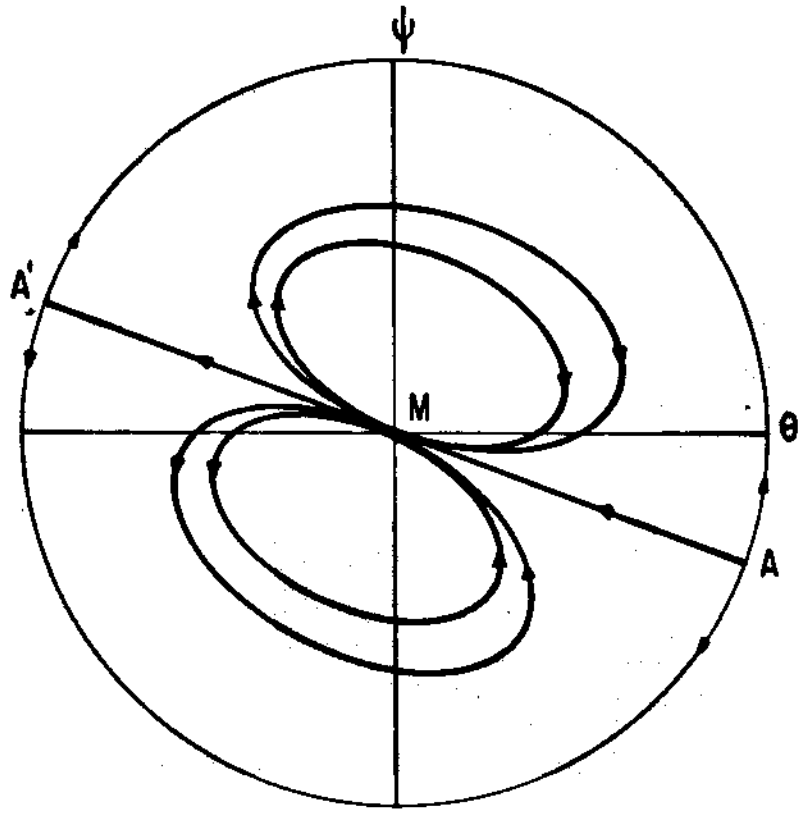

Fig.13. Dust case when $w < -3/2$.

which is an isolated equilibrium point of the system, is identified to Minkowski spacetime with static gravitational constant. The line AA' contains the invariant rays AM and MA' discussed earlier. Looking into the diagram of fig.13 we may classify the solutions basically in three distinct groups:

i) Solutions lying on the invariant ray AM.

This type of solution describes a universe starting from an initial 'big bang' ($\theta = +\infty, \psi = +\infty, \rho = +\infty$) and approaching, as the cosmic time goes by, Minkowski spacetime M. An essential feature of the models represented by this curve is that, during their whole evolution the gravitational "constant" G

increases ($\psi < 0$). So, these models do not satisfy Dirac's hypothesis, which asserts that G must decrease as the universe expands.

ii) Solutions which go from M to A'

These solutions represent cosmological models starting from Minkowski spacetime at the infinitely distant past ($t=-\infty$) going through a contraction regime until reaching final collapse. Although constant at the beginning of the cosmos, the gravitational constant decreases continuously further. Among all solutions of the diagram, this is the only one which does not end in the Minkowski spacetime M.

iii)Non-singular solutions.

The closed curves appearing in the diagram represent non-singular cosmological models starting at the infinitely distant past ($t\rightarrow-\infty$) from Minkowski spacetime and returning to it later, in the infinitely distant future. The energy density ρ (see eq.4) remains finite all the time, although it is not constant during the evolution of these universes. A typical closed trajectory undertakes initially a contraction phase with decreasing gravitational constant , followed by an expansion era (still with decreasing G) ,afterwhat the gravitational constant begins to increase , approaching a constant value as the universe tends to a Minkowskian world. Since $w < -3/2$ there is no solution in the diagram of fig.13 with $\rho < 0$.

Let us examine the next diagram, which holds for the interval $-3/2 < w < -4/3$ (fig.14).

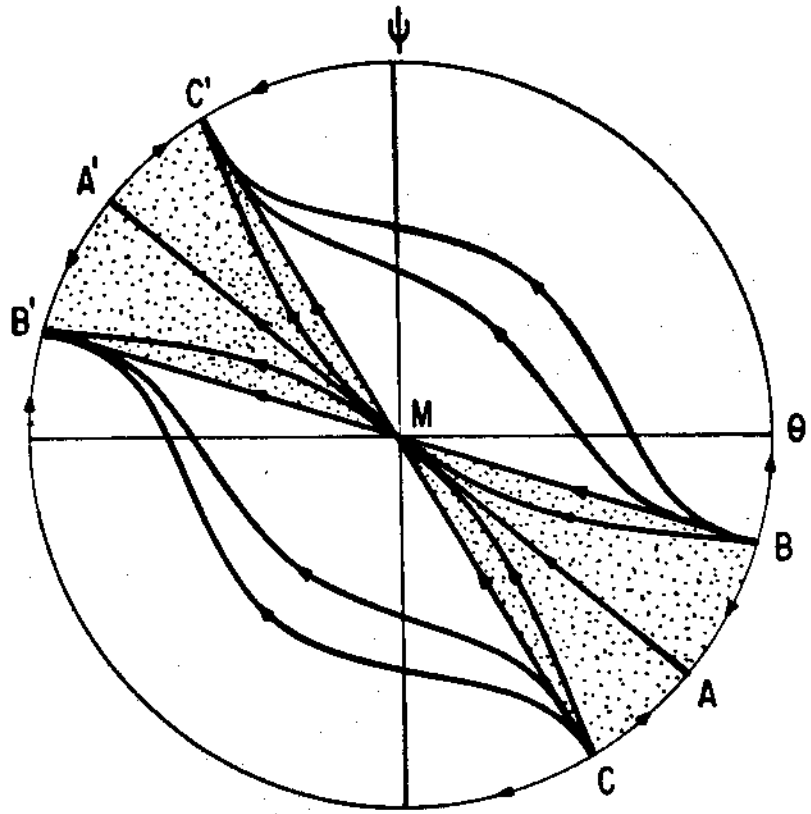

Fig. 14. Dust case with $-3/2 < w < -4/3$.
Dotted regions represent unphysical solutions with $\rho<0$.

In the above diagram ,we are left with six invariant rays : AM, MA', BM, MB', CM and MC'. As we have pointed earlier, the subdivision of two invariant rays (AM and MA') in six takes place when w reaches the value -3/2. The dotted regions in the diagram stand for solutions with $\rho<0$. At least classically, curves lying on these regions cannot describe physical models (the curves AM and MA'belong to this set) .On the other hand, solutions lying on the lines BB' and CC' (i.e., BM, MB', CM, MC') are vacuum solutions ($\rho=0$) and present singularities in their geometries, constituting 'big bang ' models (BM,CM) or collapsing models (MB', MC'). It is interesting to notice that all solutions with $\rho < 0$ necessarilly converges to or diverges from Minkowski spacetime.

Solutions lying on the sectors BMC' and CMB', which startfrom an initial explosion ($\theta = +\infty$), have an expansion phase followed by contraction and collapse in the end. They do not approach Minkowski spacetime (nor in the future, nor in the past), even though they tend asymptotically to the vacuum solutions MB' and MC'.

Let us consider the diagram corresponding to $-4/3 < w < -1$ (fig.15).

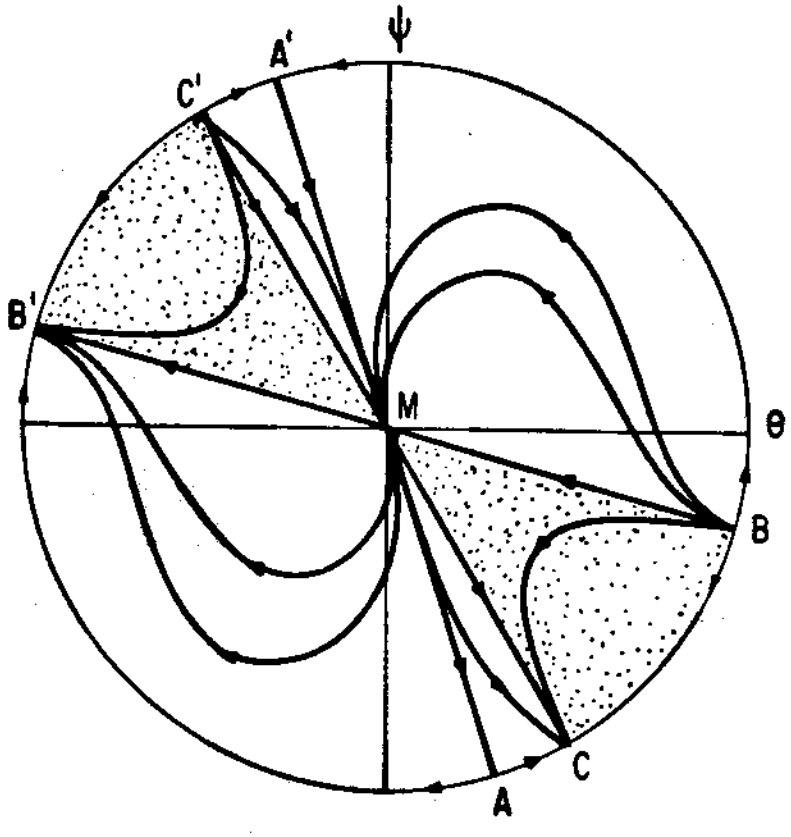

Fig. 15. Dust case with $-4/3 < w < -1$.

After passing the value w = -4/3 , the picture changes drastically. First, the curve CM reverses the direction of time, giving rise to an interesting consequence : Minkowski spacetime, as well as the vacuum solutions, are absolutely unstable with respect to negative perturbations of the energy density ρ ($\rho \rightarrow \rho + \delta\rho$, with $\delta\rho < 0$).(Instability properties of Minkowski spacetime will be discussed later). Also, when w >-4/3, AA' now lies outside the negative energy density sectors (dotteds region) , while the arrow of time reverses its direction. Thus, MA represents a model coming from a Minkowskian primordial era beginning to expand indefinitely. Since MA lies in a region where $\rho>0$, we have energy-matter being created continuously in this case. A'M, in turn, represents a contracting model which approaches Minkowski spacetime with an energy-matter annihilation process taking place. Solutions lying on sector BMA' are of 'big bang' type and go over to Minkowskian geometry (all have $\rho>0$, increasing G at the beginning and decreasing G at the final stage of their evolution.). Sector AMB' contains solutions which evolve exactly the opposite way. Solutions leaving M and terminating at C differ from MA in that they tend to the vacuum solution MC in the infinitely distant future ($t \rightarrow +\infty$) . A similar comment is valid with respect to the difference between the set of curves lying on sector A'MC' and the curve A'M. When w >-4/3 , two cases deserve a separate analysis: w = -1 and w = 0 (see figs.16 and 17 below).

If we compare fig.16 with fig.15 , we observe that the topology of the curves in these phase portraits has not been modified[5]. Yet, from the point of view of Cosmology the position of line AA' in fig.16 (w = -1) brings something anew. Observing

that AA' coincides with the ψ-axis, we conclude that the models

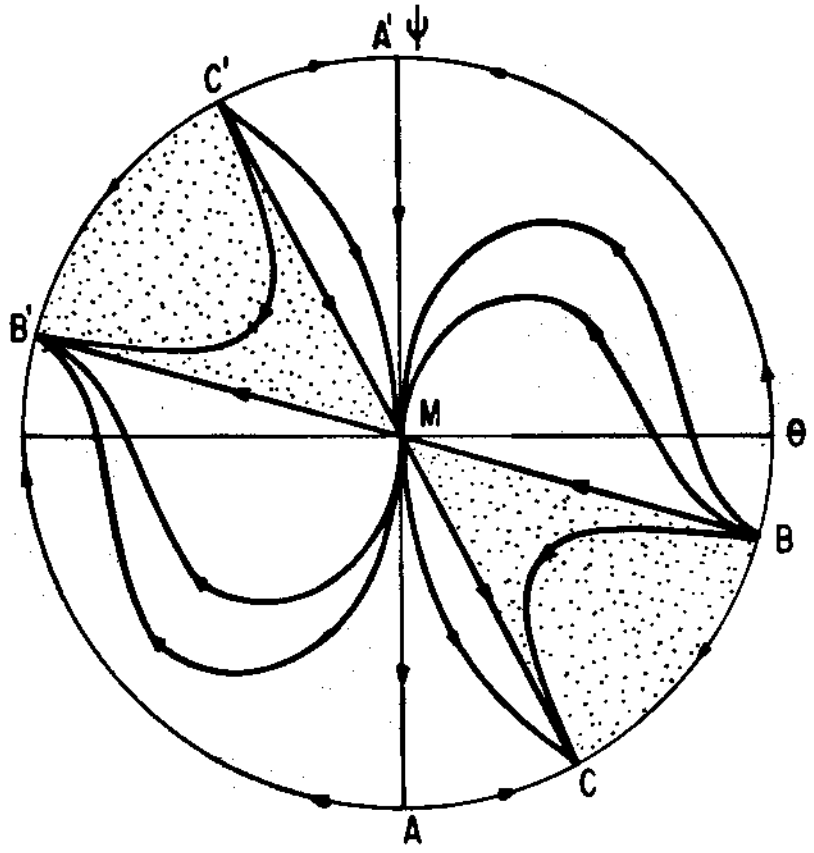

Fig.16. 'Dust' case with w = -1.

represented by the curves MA and A'M are static models (θ = 0). So, we have static spacetimes (Minkowskian geometry) with a varying gravitational constant and positive energy density. Models represented by the curve AM (A'M) in fig.16 leaves (tends to) Minkowski spacetime (where we have θ = 0 , ψ = 0 and ρ = 0); so, we have creation (annihilation) of matter in these models.

Let us examine the case w = 0 (fig.17). Here, the static solutions lying on CC' are vacuum solutions with varying G. Thus, we are in presence of a varying scalar field ϕ which is not generated by any external matter field. This fact violates the usual formulation of Mach's principle[1]. On the other hand, in

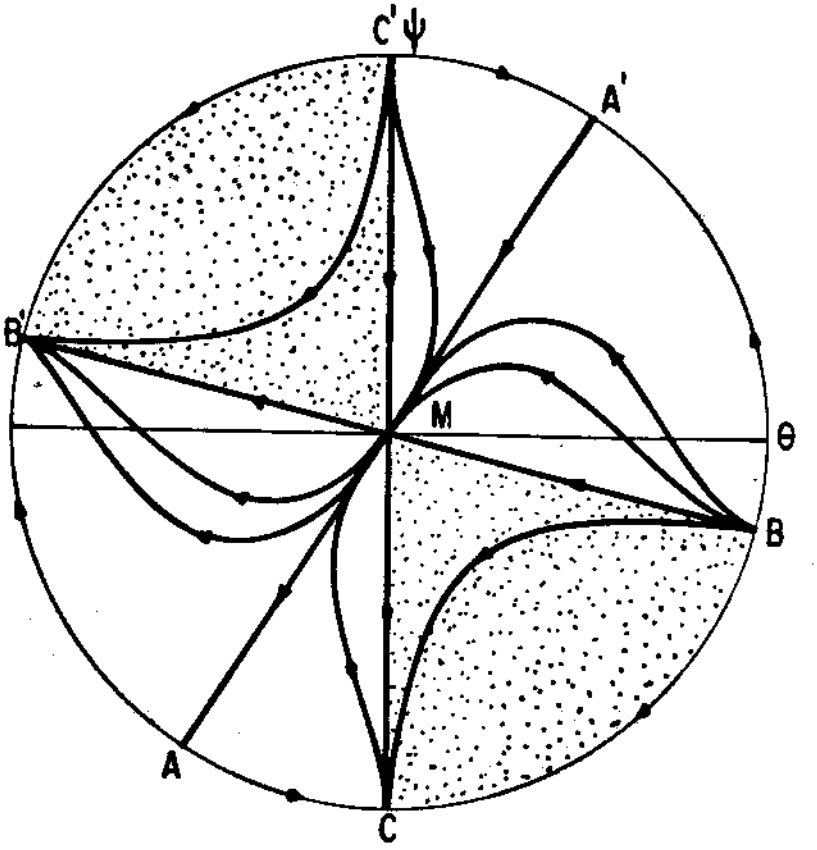

Fig.17. 'Dust' solutions for w = 0.

fig.16 and fig.17 there appear what could be claimed to be the "best" solutions of Brans-Dicke theory: those which represent 'big bang' expanding models ($\theta > 0$) having positive energy density and a gravitational constant that satisfies Dirac's hypothesis. We are refering to the class of solutions described by the curve A'M. As we shall see further, except for radiation ($\lambda = 1/3$) and stiff matter cases, this kind of solution is available for all values of λ in a certain definite range of variation of w. That is, for dust models this happens when $w > -1$; for $0 < \lambda < 1/3$, when $w > \frac{1}{\lambda - 1}$; for $1/3 < \lambda < 1$, when $w < \frac{1}{\lambda - 1}$. Solutions lying on MA are just the 'counter-part' of those on A'M and do not have so

much physical interest since they have opposite properties of A'M. At this point, we call attention also for solutions of sector C'MA' : these are all non-static solutions having positive energy density , decreasing gravitational constant and approaching Minkowski spacetime as $t \to \infty$ .Curves on sector MAC,in turn, do not describe physically appealing cosmological models .

When $w > 0$ (see fig.18) the only significant fact we should comment on is that the vacuum solutions represented by C'M and MC are not static solutions anymore (as in fig.17).

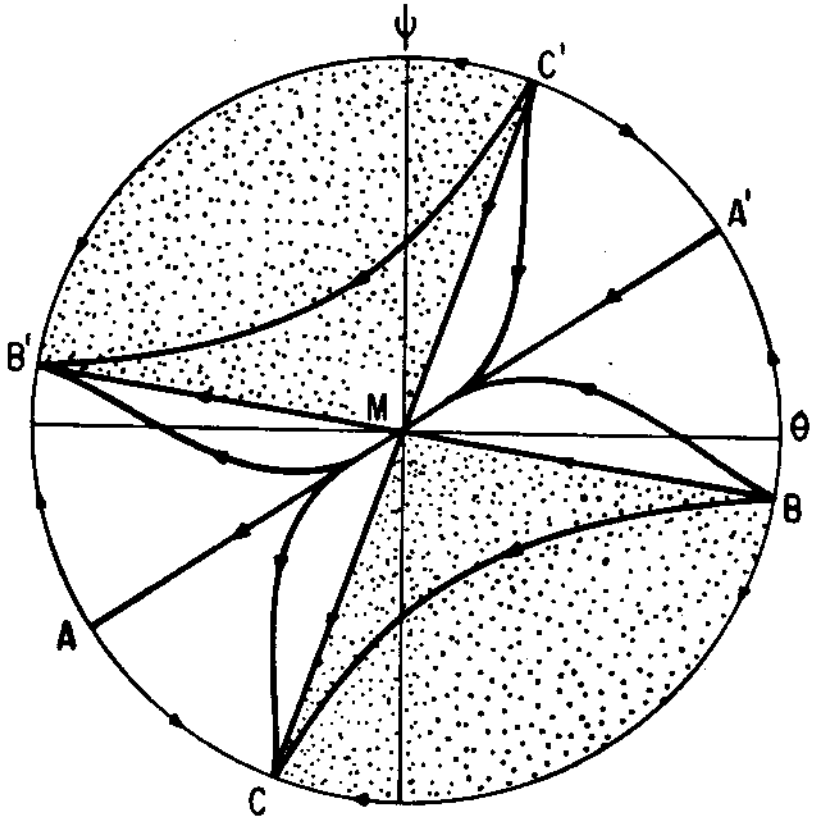

Fig.18. Dust case with $w > 0$.

Finally, as w becomes large , the "forbidden" regions, i.e., regions where the energy density is negative (sectors MB'C'

and MBC), become wider, as we have pictured in figs.2 and 3. However, the line A'A still remains in the positive region. When $w \to +\infty$ the solutions with $\rho > 0$ go over the Friedmann dust solution represented in fig.19 as lying on the line AA', which is in accordance with the known fact that Brans-Dicke theory tend to general relativity when w becomes large.

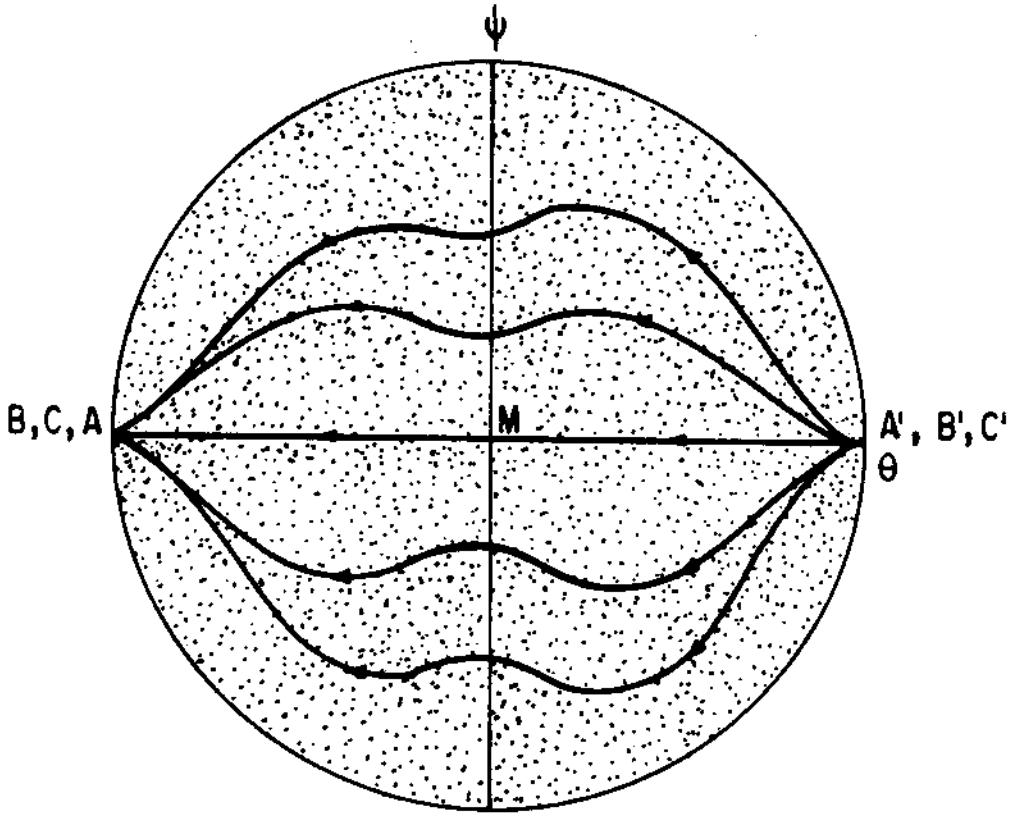

Fig.19. Dust solutions when $w \to +\infty$.

b) *The radiation case*

It is a well known fact that in Brans-Dicke theory when the fluid obeys the equation of state $p = (1/3)\rho$, the scalar field

ϕ is sourceless (which is readily seen from eq.(1.b) since T=0). This means that Einstein's radiation solutions will satisfy Brans-Dicke field equations (1.a) and (1.b) if we take $\phi = G^{-1} =$ const. It is interesting to see that this result may be deduced simply by looking into the phase portraits for $\lambda = 1/3$ (see figs.20,21 and 23). Indeed, in this case the line AA' which contains the two invariant rays AM and MA' is fixed (it does not depend upon the value of the coupling constant w and, thus, does not rotate in the phase plane as w varies) and coincides with the θ-axis. Friedmann's radiation solution

$$R = Rot^{1/2} \quad , \quad \phi = G^{-1} \quad , \quad \rho = \frac{3G}{32\pi t^2}$$

lies on the curve AM.

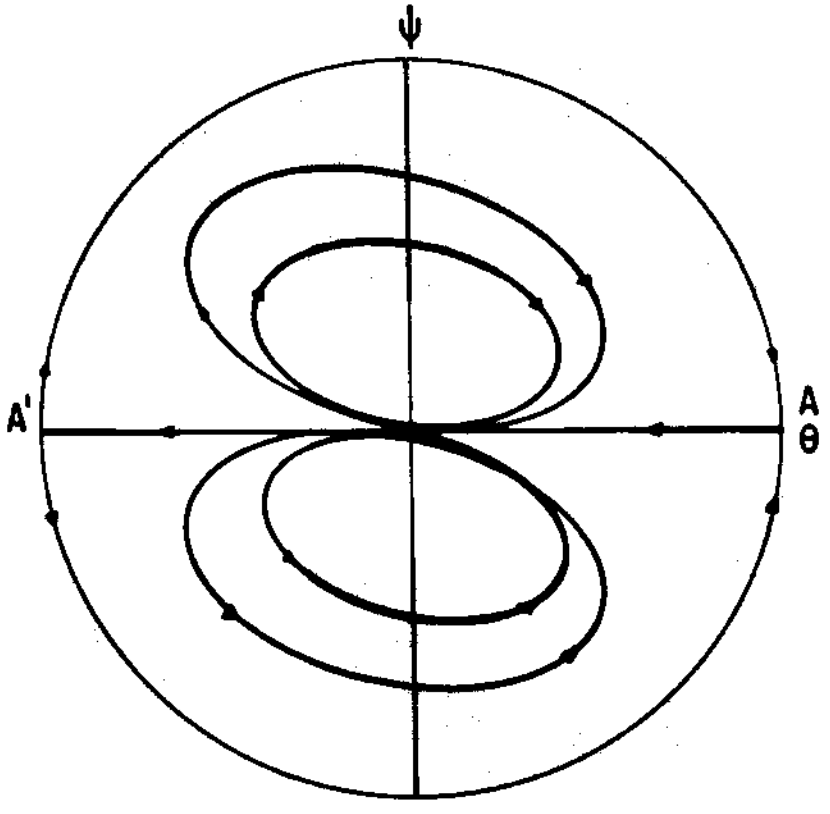

Fig. 20. Radiation case with $w < -3/2$. There is no region with $\rho<0$.

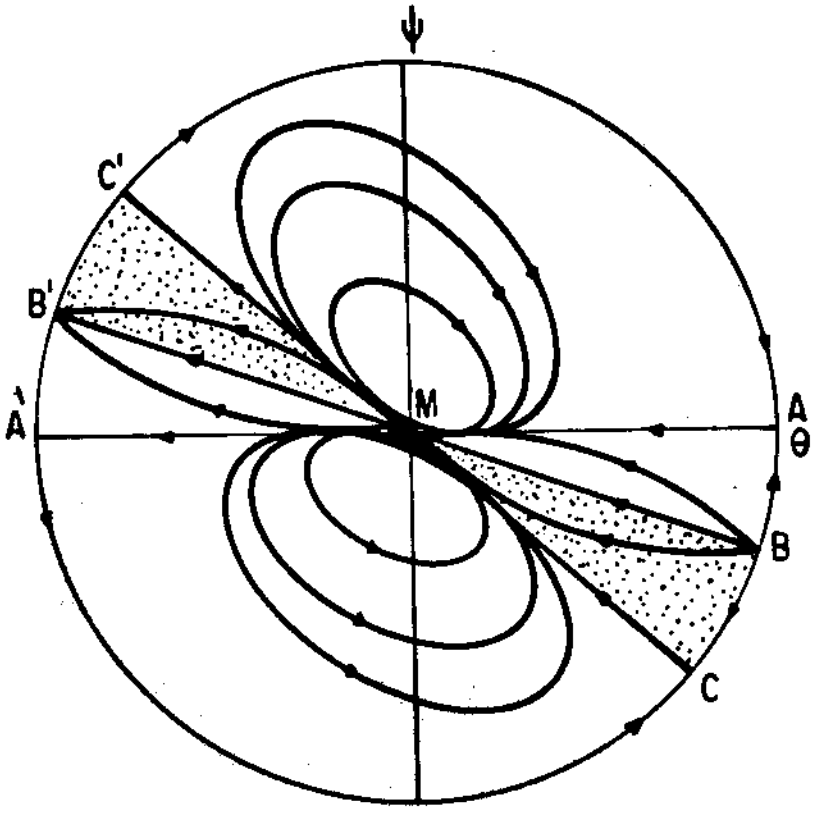

Fig. 21. Radiation case with $-3/2 < w < -4/3$.

The comments we made on the dust case hold also for the majority of solutions of the phase diagrams in the radiation case. Nevertheless, let us examine some new characteristics occurring in figs. 20, 21 and 22:

If $w < -3/2$, fig. 20 shows that we have almost the same pattern of fig. 13., the only difference being the existence of singular solutions with non-varying G.

In fig. 21 ($-3/2 < w < -4/3$) we identify closed curves representing non-singular solutions lying on the region where $\rho > 0$. This does not violate Hawking's theorems on singularities since the strong energy condition $\tilde{T}_{\mu\nu} V^\mu V^\nu \geq \tilde{T}/2$ is not fulfilled by these solutions in the interval $-3/2 < w \leq -4/3$, where here $\tilde{T}_{\mu\nu}$

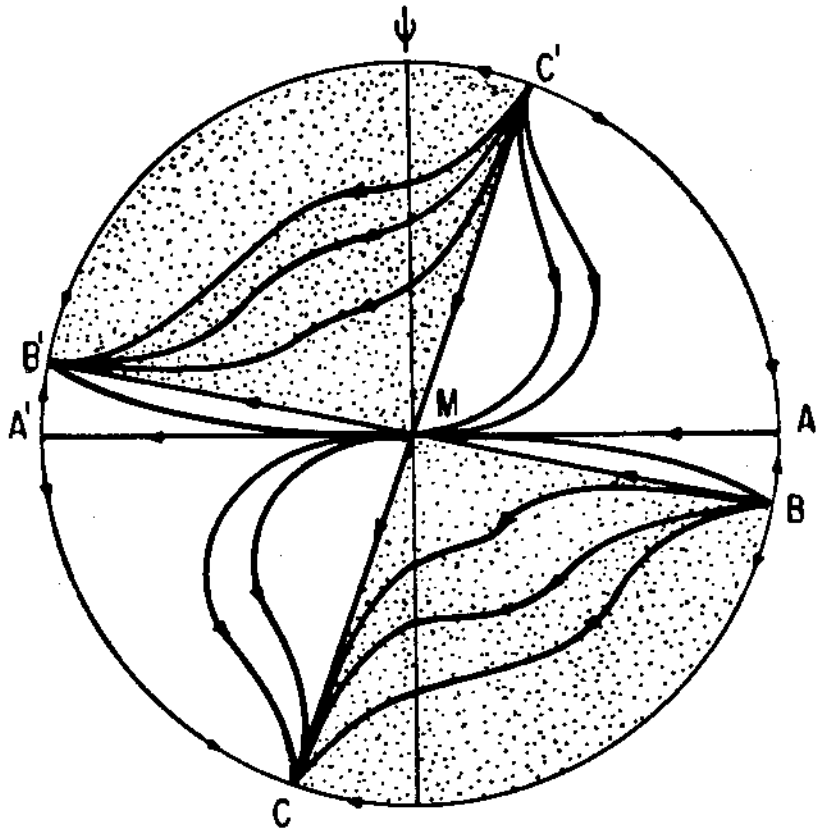

Fig. 22. Radiation case with w > 0.

denotes the energy-momentum tensor in the revised Dicke version[7]. Actually , this explains the occurrence of non-singular solutions for w =-4/3 found out by O'Hanlon and Tupper[13].

When w > -4/3 we do not have non-singular solutions anymore. Incidentally, this result holds for all cases we will analyse later. The curve C'M which appear in fig.22 (w > 0) is essentially the same of the dust case when w > 0 (see fig.18), except that, here, solutions represented by this curve tend asymptotically to Friedmann solution lying on AM.

c) The case $0 < \lambda < 1/3$.

This case is an intermediary between dust and radiation. The rotation of the invariant ray AA' is depicted in figs.7-9 and is identical to the dust case. Almost the totallity of the diagrams when $0 < \lambda < 1/3$ look like the dust diagrams. However, besides the values $w = -3/2$ and $w = -4/3$, there are also topological changes i the phase plane when w takes the values $w = w^{*}(\lambda) = \frac{2\lambda-4/3}{(\lambda-1)^2}$ and $w = w^{**}(\lambda) = 4/3(\lambda^2-1)$. These new critical points $w^{*}(\lambda)$ and $w^{**}(\lambda)$ are present too in the case $1/3 < \lambda < 1$. When $0 < \lambda < 1/3$ the following inequality holds: $-3/2 < w^{*}(\lambda) < w^{**}(\lambda) < -4/3$ .It is worthwhile noticing that if $\lambda = 0$, then $w^{*}(\lambda) = w^{**}(\lambda) = -4/3$ and when $\lambda = 1/3$, then $w^{*}(\lambda) = w^{**}(\lambda) = -3/2$.

The diagrams for $1/3 < \lambda < 1$ and $w < -3/2$ are identical to fig.13. Also, when $-3/2 < w < w^{*}(\lambda)$ we have the same diagram as infig.14. The analysis of thes two cases has been carried out before. Now, when $w^{*}(\lambda) < w < w^{**}(\lambda)$ we obtain the following configuration:

Looking at the diagram of fig.23 we see that the curve AM lies on a region of positive energy density representing 'big bang' models with increasing gravitational constant. We do not have a model with such characteristic in the cases analysed previously. A similar comments can be made on the solutions contained in MA' which describe collapsing universes with decreasing G starting from a Minkowski era. Solutions which come from B and go to A' are also new : asymptotically they begin as vacuum solutions undergoing an expansion phase , followed by contraction and finally entering into a process of collapse towards the singularity with an infinite energy density. AB'

models behaves the reverse of BA' models.

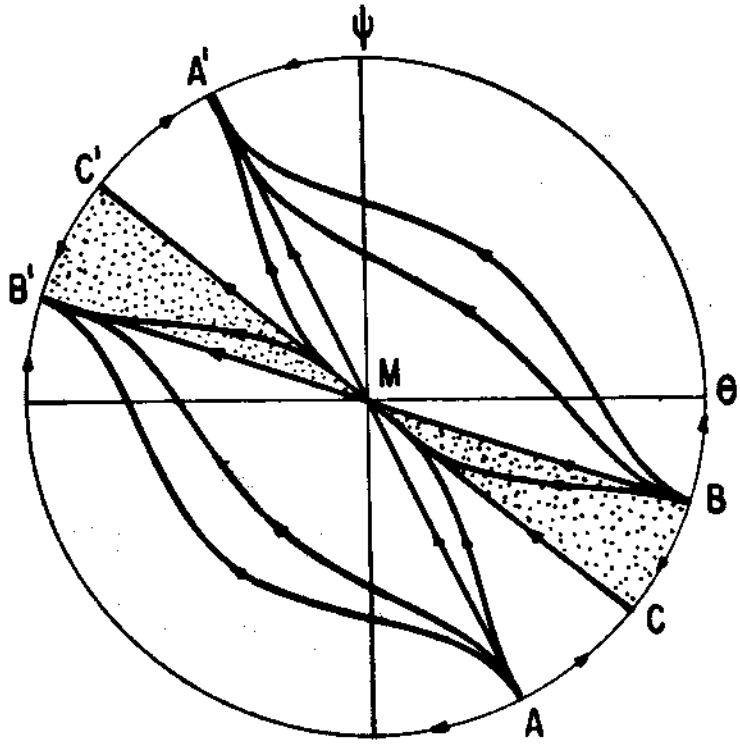

Fig. 23. Case $0 < \lambda < 1/3$ and $v^{*}(\lambda) < v < v^{**}(\lambda)$

Let us consider $w^{**}(\lambda) < w < -4/3$ (see fig.24).

Here, we find closed solutions which are not similar to those appearir in the radiation case when $-3/2 < w < -4/3$ (see fig.21). The non-singular solutions of fig.24 are always contracting or always expanding (non-singular solutions disappear when $w > -4/3$). We must observe also that A'M and MA have changed their orientation in time if we compare this configuration with the former diagram (see fig.23).

Static solutions (analogous to the dust case) are obtained when we set $w = \frac{1}{\lambda-1}$. This value of w is greater than $w^{**}(\lambda)$ when $0 < \lambda < 1/3$. The phase diagram corresponding to w =

$\frac{1}{\lambda-1}$ is identical to that of fig.16. When $w = 0$ and $w > 0$ we

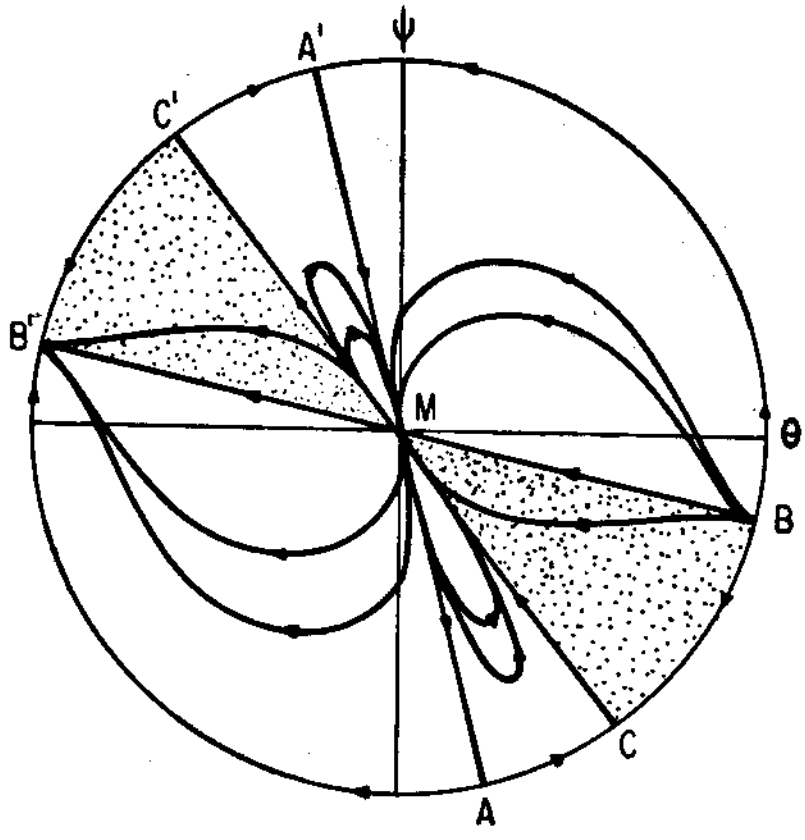

Fig. 24. Case $0 < \lambda < 1/3$ and $v^{**}(\lambda) < v < -4/3$.

obtain phase diagrams identical to those obtained in the dust case for the same values of w(see figs.17 and 18, respectively). We should point out once more that in both cases ($w = 0$ and $w > 0$) the most significant curves are, as for dust models, those lying on the invariant ray A'M or those lying on the sector A'MC'. As we have seen before, these curves represent 'big bang' models with decreasing gravitational constant and positive energy density. The evolution of the phase diagrams as $w \to +\infty$ is the same as in the dust case ; hence, all we have stated in section 4.a is valid also for the case $0 < \lambda < 1$.

d) *The case 1/3 < λ < 1.*

Let us take up the case when the fluid obeys an equation of state $p = \lambda\rho$ with λ in the interval $1/3 < \lambda < 1$, which is an intermediary between radiation and stiff matter. As the the sense of rotation of the line AA' is concerned, we notice now that it is counterclockwise (see figs. 10-12). On the other hand, in this case, $w^{**}(\lambda) < -3/2$; and $-3/2 < w^{*}(\lambda) < -4/3$ if $\lambda < 1/2$ or $w^{*}(\lambda) \geq -4/3$ if $\lambda \geq 1/2$. So, in a certain range of variation of w, we have to distinguish the phase diagrams according to whether $\lambda<1/2$ or $\lambda \geq 1/2$.

When $w < w^{**}(\lambda)$ (and $1/3 < \lambda < 1$) we have three diagrams corresponding to: 1)$w < \frac{1}{\lambda-1}$ (fig.25), $w=\frac{1}{\lambda-1}$(fig.26) and $\frac{1}{\lambda-1} < w < w^{**}(\lambda)$ (fig.27).

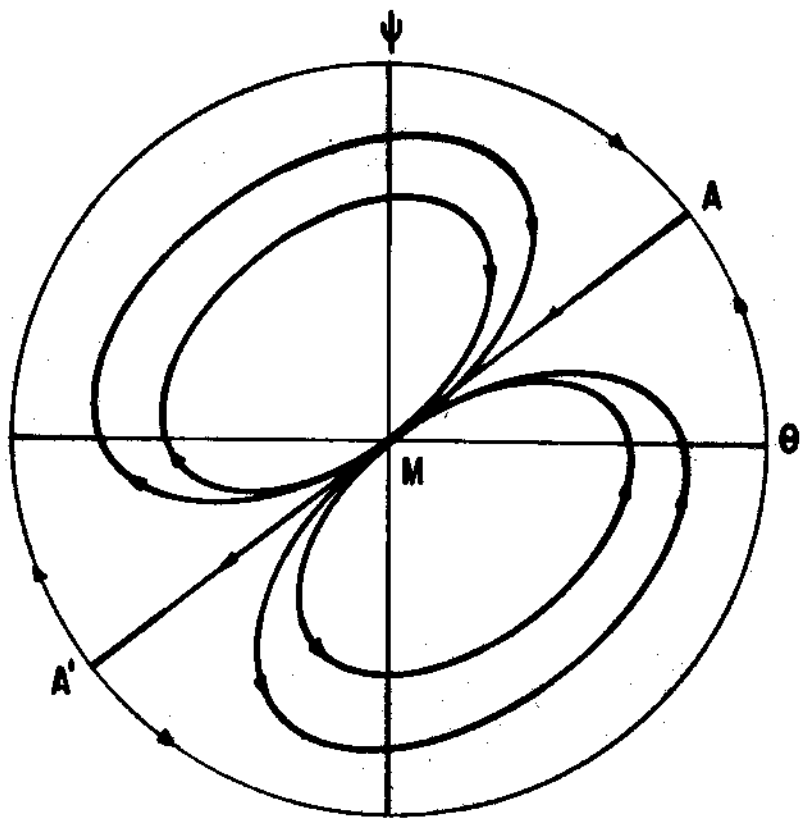

Fig. 25. $1/3 < \lambda < 1$ and $w < \frac{1}{\lambda-1}$.

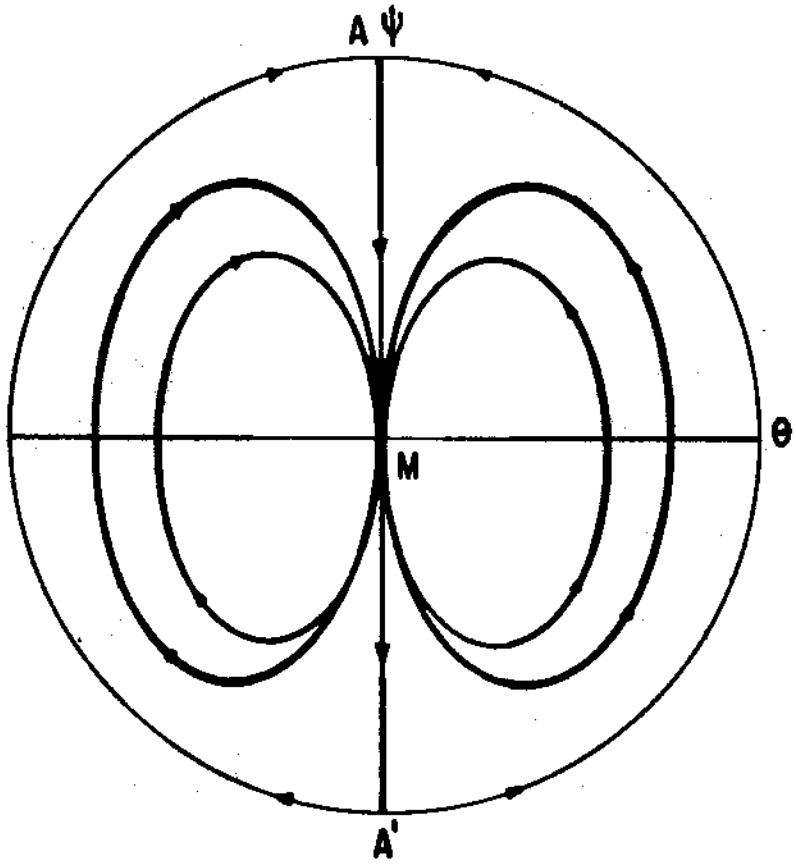

Fig. 26. $1/9 < \lambda < 1$ and $w = \frac{1}{\lambda - 1}$.

In the first of these diagrams (fig. 25) we have closed (non-singular) solutions and also singular solutions (lying on AA'). As we have discussed earlier, AM represents cosmological models exhibiting physical properties quite desirable to anymodel intending to fit observational data. Nevertheless, this solution exists only for $w < \frac{1}{\lambda - 1}$, i.e., for negative w, thus contradicting arguments which restrict w to be positive[2].

In the diagram of fig. 26 AM and MA' are static solutions with $\rho > 0$, already discussed in section 4.a. The closed solutions here are of two types: expanding models or

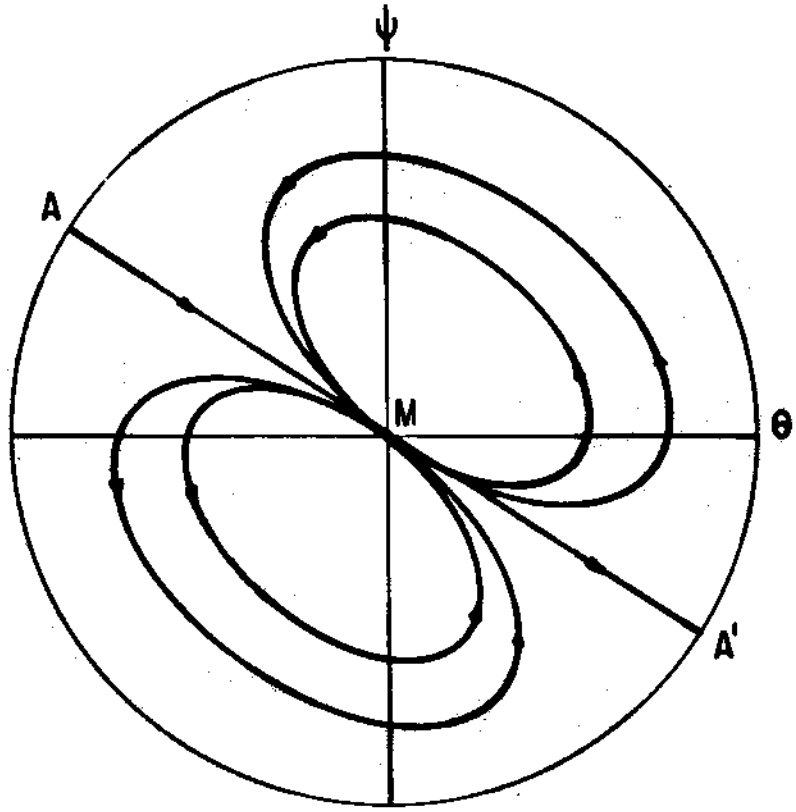

Fig. 27 $1/3 < \lambda < 1$ and $\frac{1}{\lambda-1} < v < v^{**}(\lambda)$.

contracting models, both everlasting universes approaching Minkowski spacetime. The gravitational constant in these models increases during a period of time and,then, start decreasing. In fig.27 we have the same solutions of the dust case, but now with direction of time reversed (see fig.13).

Let us investigate the diagram corresponding to the case $w^{**}(\lambda) < w < -3/2$ (fig.28) . The solutions lying on AA' change their original direction of time and the closed solutions become singular 'big bang' models collapsing in the future. We have already found solutions somewhat similar to these in the investigation of the dust case (fig.14) and also when $0 < \lambda < 1/3$ (fig.23) , although there the solutions either originated from

or tended asymptotically to vacuum solutions (see fig.23).

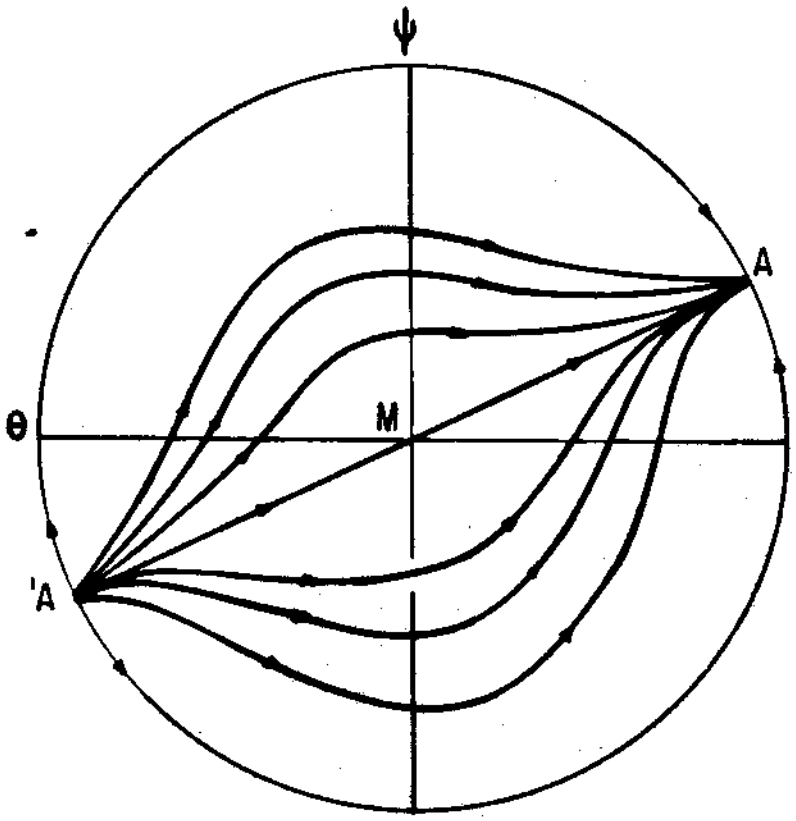

Fig. 28. Case $1/3 < \lambda < 1$ and $v^{**}(\lambda) < v < -3/2$.

To continue, at this point we have to divide our analysis according to whether $1/3 < \lambda < 1/2$ or $1/2 \leq \lambda < 1$. In the first possibility, there are three topologically distinct cases: $-3/2 < w < w^{*}(\lambda)$, $w^{*}(\lambda) < w < -4/3$ and $w > -4/3$. In the second possibility, the distinct cases to be examined next are: $-3/2 < w < -4/3$ $-4/3 < w < w^{*}(\lambda)$ and $w > w^{*}(\lambda)$.

So, let us assume initially that $1/3 < \lambda < 1/2$ and consider fig.29, which corresponds to $-3/2 < w < w^{*}(\lambda)$:

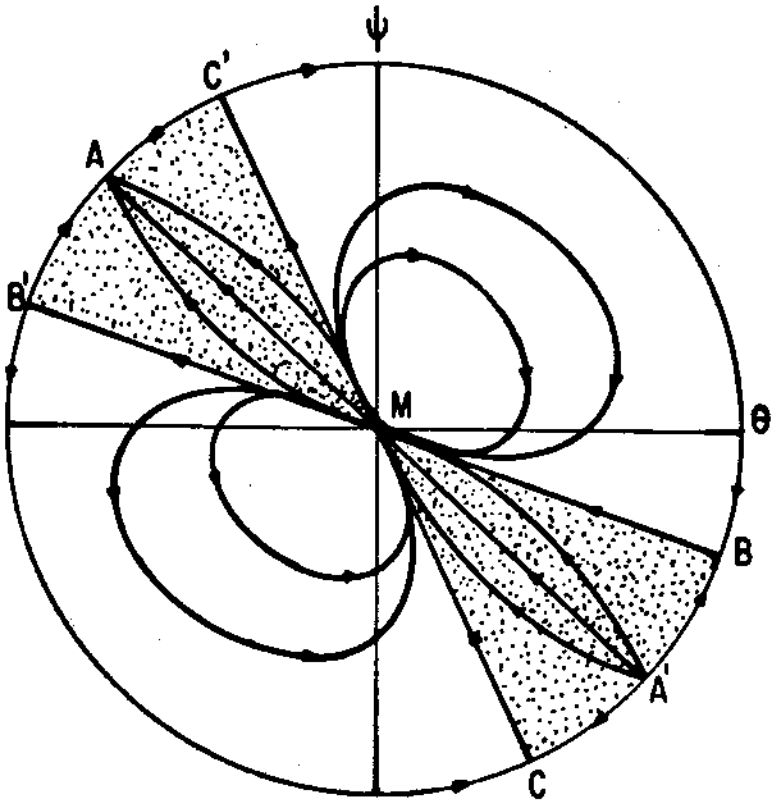

Fig. 29. Case $1/3 < \lambda < 1/2$ and $-3/2 < w < w^{*}(\lambda)$.

In the figure above there appear the vacuum solutions BM, MB', CM and MC'. Solutions lying on the regions BCM and B'C'M' have negative energy density and look like those of fig.14. lying on the same regions, although they do not approach vacuum solutions near the singularity. Only the closed solutions in this diagram have positive energy density.

When $w^{*}(\lambda) < w < -4/3$ (see fig.30) the curve A'M emerges in the region where where $\rho > 0$, representing expanding 'big bang' models with increasing gravitational constant. This type of solution has been already alnalysed before when we

considered the dust case (see fig.13).

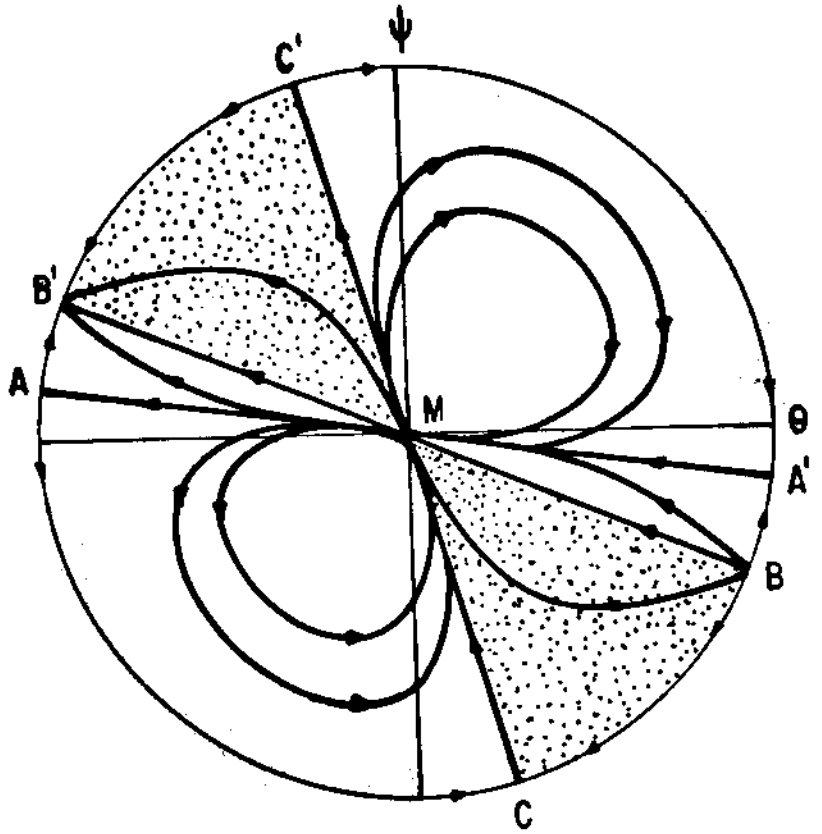

Fig. 30. Case $1/3 < \lambda < 1/2$ and $v^{*}(\lambda) < v < -4/3$.

If w lies in the interval $-4/3 < w < 0$, we have the diagram of fig.31.

At the value $w = 0$ the line CC' coincides with the ψ-axis and then we obtain the static vacuum solutions already discussed (see, for instance, fig.17).

For $w > 0$ the corresponding phase diagram is depicted in fig.32.

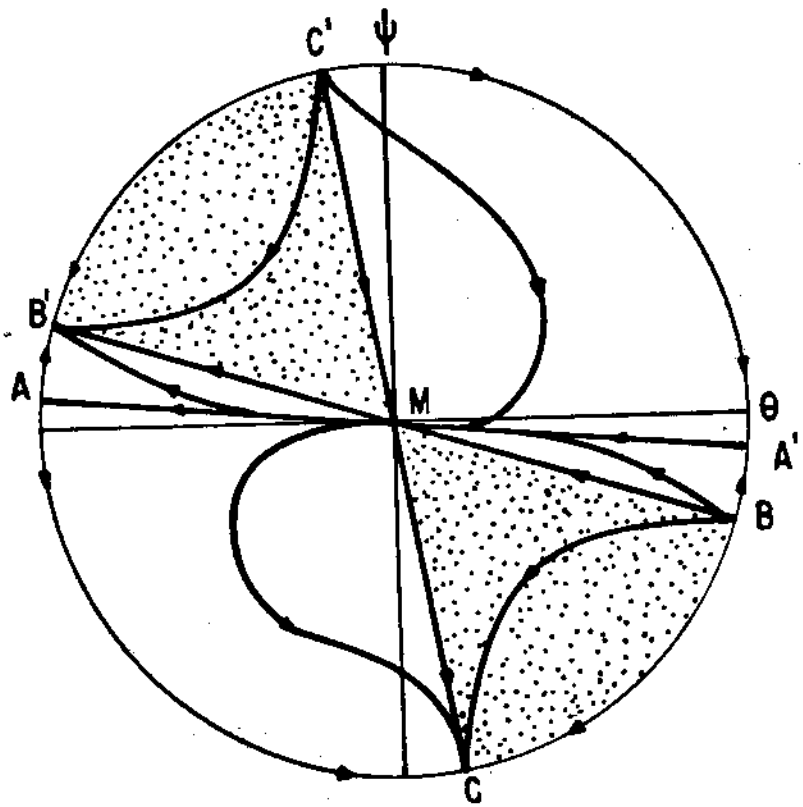

Fig. 31. Case $1/3 < \lambda < 1/2$ and $-4/3 < \nu < 0$.

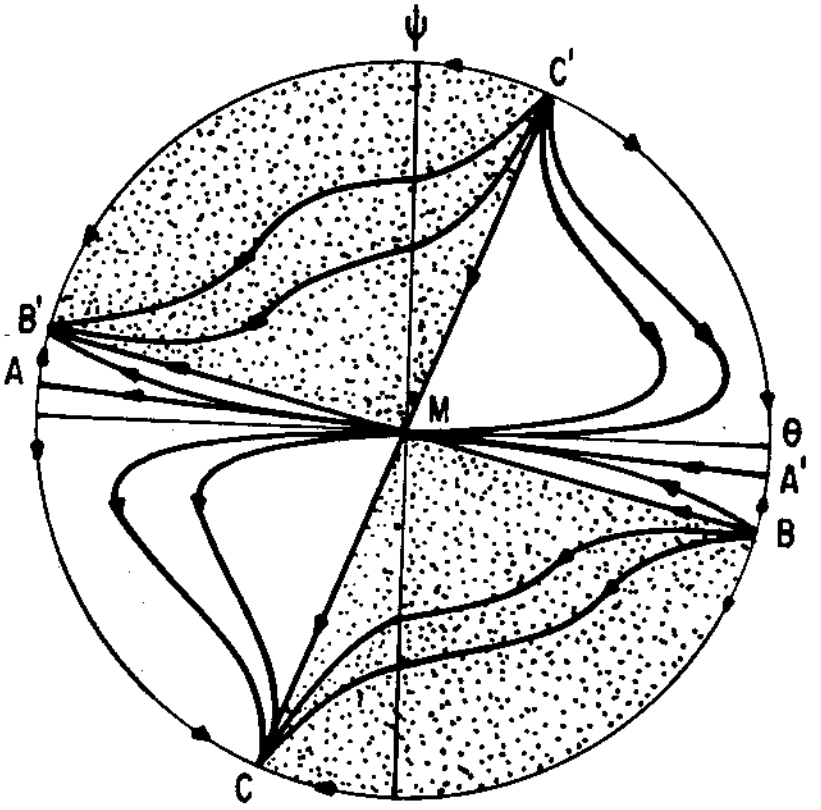

Fig. 32. Case $1/3 < \lambda < 1/2$ and $w > 0$.

It should be mentioned that the later three diagrams are topologically equivalent in the plane phase.

Now, let us suppose that $1/2 < \lambda < 1$. If $-3/2 < w < -4/3$ we will have exactly the same diagram of fig. 29., and for $-4/3 < w < w^{*}(\lambda)$ we will obtain the diagram of fig. 33.

Finally, when $w > w^{*}(\lambda)$ and also in the limit $w \to +\infty$ we obtain again the same diagrams as in figs. 32 and 19, respectively.

e) *The stiff matter case.*

The next case to be examinated is of a fluid with the stiff matter equation of state $p = \rho$. Five diagrams are

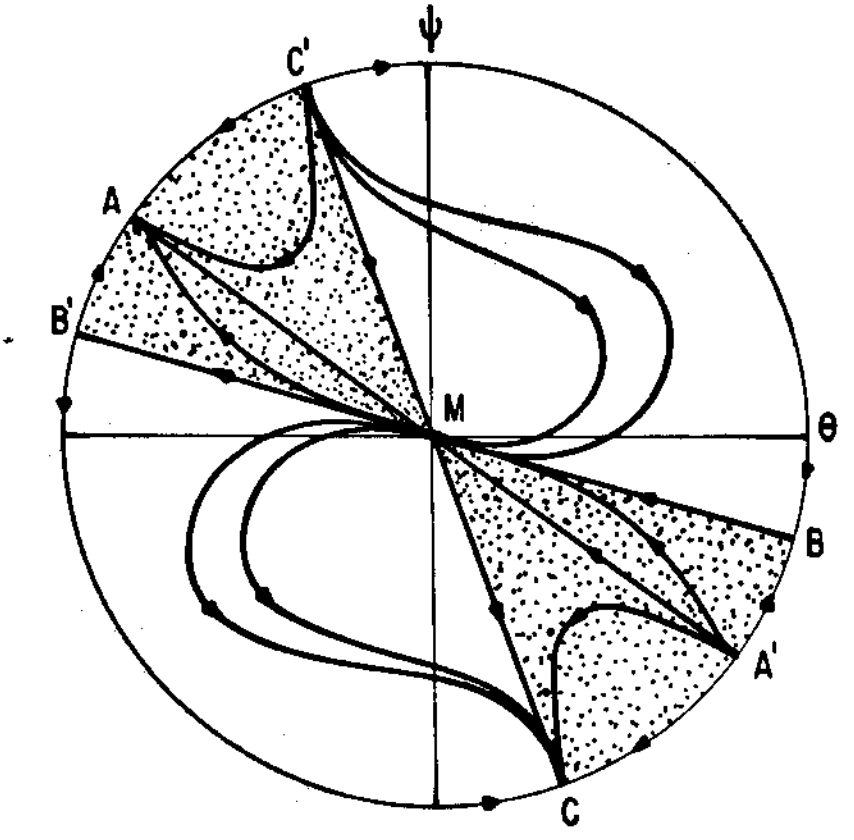

Fig. 33. Case $1/2 < \lambda < 1$ and $-4/3 < w < w^{*}(\lambda)$.

necessary for complete characterizing this case: $w < -3/2$ (fig. 34), $-3/2 < w < -4/3$ (fig. 29), $-4/3 < w < 0$ (fig. 35), $w > 0$ (fig. 36) and $w \to +\infty$ (fig. 37).

Initially, we should mention that if $\lambda = 1$ the line AA' does not rotate in the phase plane $\theta\psi$ as w takes different values. In fact, AA' is fixed and makes an angle $\alpha = -33.69^{\circ}$ with the positive θ-axis.

When $w < -3/2$, in contrast to the previous cases, we have no closed curves in the diagram. Instead, we have only expanding 'big bang' models with a subsequent contraction phase (see fig. 34).

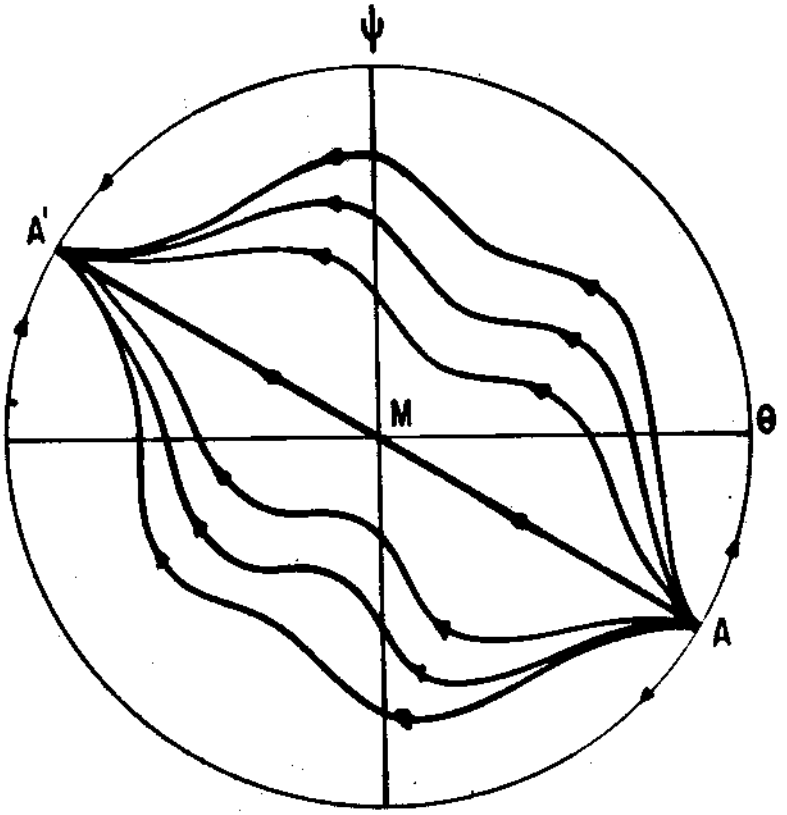

Fig. 34. Stiff matter case with $w < -3/2$.

On the other hand, when $-3/2 < w < -4/3$ the portrait is equal to that of fig. 29. In the interval $-4/3 < w < 0$ we get the diagram of fig. 35.

The next diagrams correspond to $w > 0$ (fig. 36) and to $w \to +\infty$ (fig. 37).

It should be pointed out that in the stiff matter case the solutions corresponding to the invariant rays AM and MA' have positive energy density only when $w < -3/2$ and that non-singular solutions are permitted only in the interval $-3/2 < w < -4/3$. When $w \to +\infty$ all solutions with $\rho > 0$ tend to the vacuum solutions represented by BM (or C'M) and MB' (or MC).

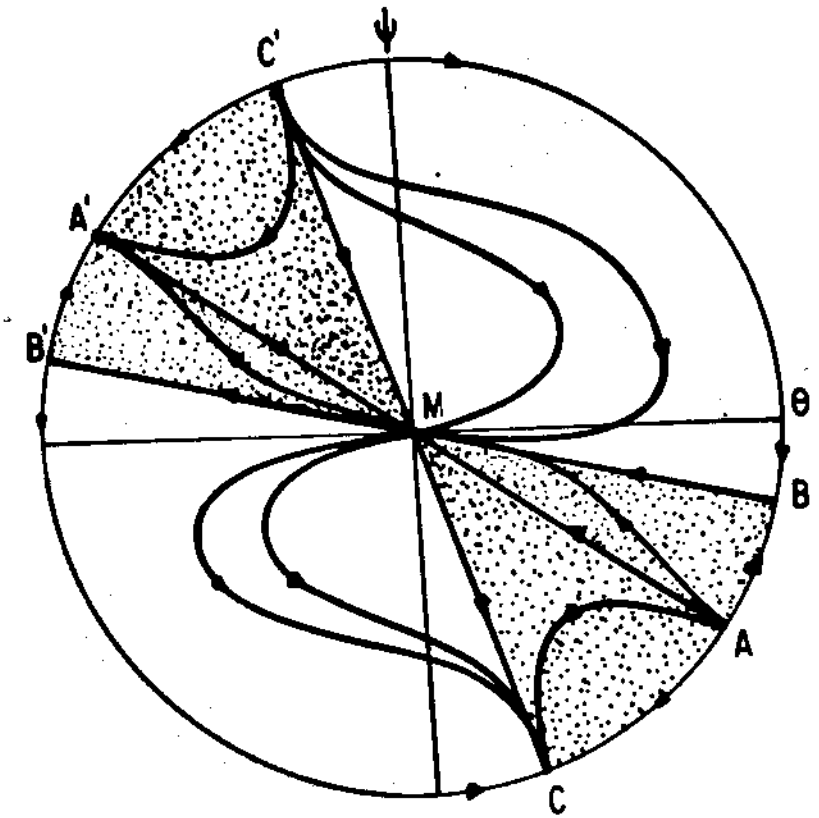

Fig. 35. Stiff matter case with $-4/3 < \nu < 0$.

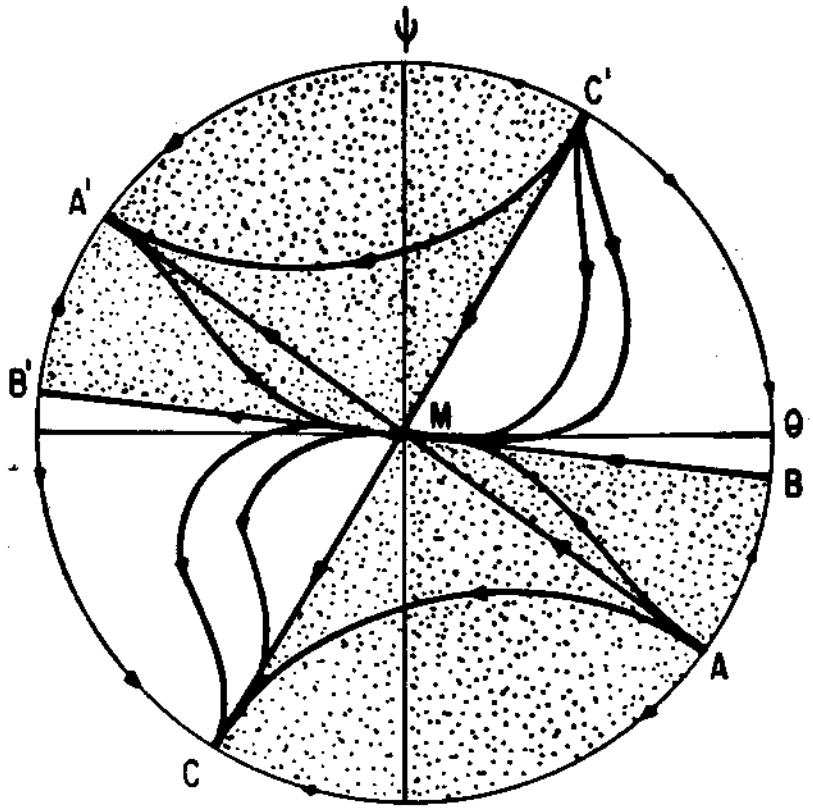

Fig. 36. Stiff matter case with $v > 0$.

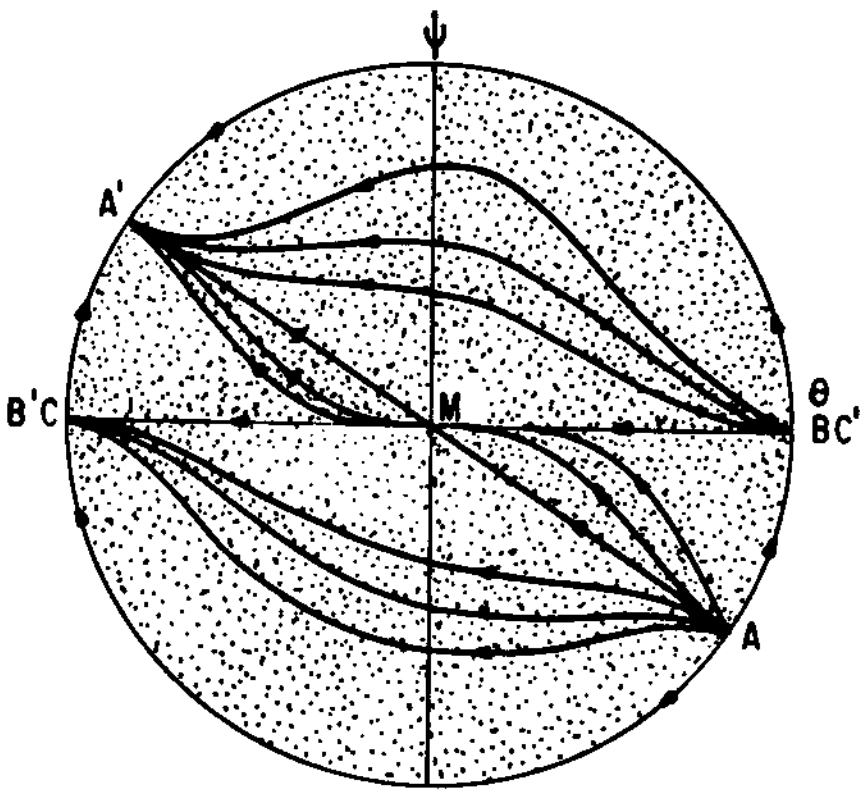

Fig. 37. Stiff matter case with $v \to +\infty$.

5. Stability properties of Minkowski spacetime in Brans-Dicke theory

It would be rather tedious to analyse the stability properties of Minkowski spacetime as well as of some solutions in Brans-Dicke theory looking into, one by one, all the diagrams presented in the preceding section. Certainly, there are some regularities amongst the phase portraits, but these regularities are not sufficient enough to allow us treating the subject in a general and simplified way. Thus, we shall restrict ourselves to considering only two diagrams which seems to us to be very typical ones.

Actually, we are interested in the stability of Minkowski spacetime which is pictured in all diagrams as the origin M of the phase plane and which constitutes the only isolated equilibrium point of the dynamical system (3). The kind of stability we are concerned with here must be understood in the usual sense of dynamical system theory: we consider solutions with initial conditions ($\theta_o = \theta(t_o)$, $\psi_o = \psi(t_o)$) lying near an equilibrium point and observe the evolution of these solutions with time.

We begin by considering fig.13 which represents the phase diagram of dust models when $w < -3/2$. This pattern is also present, as we have seen in the case of fluids satisfying the equation of state $p = \lambda\rho$ with $0 < \lambda < 1/3$. So, looking at this diagram we verify that, except for the line AA', throughout the entire phase plane Minkowski spacetime M exhibits a curious type of stability. The existence of closed curves makes Minkowski spacetime unstable in a small region near the origin M (local instability) ,though when $t \to +\infty$ any perturbation of this solution

tends to disappear since the closed curves return to M (global stability).

Now, let us turn our attention to fig.18, where we have $w > 0$ and $0 \leq \lambda < 1/3$. In this diagram we can identify three distinct regions: sector BMC', sector B'MC and the region with negative energy density (dotted areas). Let us consider sector BMC', which contains the solution A'M. Finite perturbations of Minkowski spacetime with respect to θ, ψ and ρ within this region tend to vanish as the cosmic time goes by. Thus, BMC' is a region of stability for M. Likewise, sector B'MC is a region of instability: small perturbations in θ, ψ and ρ tend to increase more and more as the perturbed models evolve in time. If we perturb Minkowski spacetime with respect to the energy density ρ in such a way that $\delta\rho<0$ (which is equivalent to going into the dotted regions), then we fall in a region of instability where the solutions run away indefinitely from M.

6. Conclusion

As it has been pointed out by some authors recently[15], the increasing use of the theory of dynamical systems as a powerful tool in the study of cosmological models lies specially on the fact that one is not restricted to isolated solutions, but, rather, there is the possibility of carrying out a general analysis of entire classes of solutions.

In this paper we have been concerned with models of the universe predicted by a particular scalar-tensor theory[16] of gravitation under assumptions of homogeneity, isotropy and spatial flatness. The diagrams we have shown cover the essentials of